An acoustic scattering model for stratification interfaces

Elizabeth Weidner and Thomas C. Weber

Citation: The Journal of the Acoustical Society of America **150**, 4353 (2021); doi: 10.1121/10.0009011
View online: https://doi.org/10.1121/10.0009011
View Table of Contents: https://asa.scitation.org/toc/jas/150/6
Published by the Acoustical Society of America

JASA ARTICLE

An acoustic scattering model for stratification interfaces

Elizabeth Weidner[a] and Thomas C. Weber
Center for Coastal and Ocean Mapping, University of New Hampshire, 24 Colovos Road, Durham, New Hampshire 03824, USA

ABSTRACT:
Stable fluid bodies, such as the ocean and atmosphere, are composed of a series of increasingly dense layers, defined by density stratification interfaces in which the medium properties (e.g., temperature, salinity) change. The intensity of the stratification between the layers influences the internal mixing dynamics and entrainment, facilitating the transport of dissolved constituents within the fluid medium. Acoustic systems offer the means for high resolution observations of these interfaces, which allow for continuous data collection over broad spatial scales. Here, a one-dimensional acoustic scattering model is presented for predicting acoustic backscatter from stratification interfaces, which is widely applicable to the acoustic water column data collected with ship-mounted sonars. Model predictions based on hydrographic profiles suggest that in many oceanic cases, the density gradient perturbations can be disregarded, and sound speed perturbations alone drive the majority of the acoustic scattering. A frequency-dependent scattering intensity based on the sharpness of the stratification interface is predicted by the model, suggesting a path to remote estimations of the physical medium properties through broadband acoustic inversion.
 https://doi.org/10.1121/10.0009011
(Received 15 July 2021; revised 20 October 2021; accepted 20 November 2021; published online 15 December 2021)
[Editor: D. Benjamin Reeder] Pages: 4353–4361

I. INTRODUCTION

Stable fluid bodies, such as the atmosphere and much of the ocean, are composed of a series of increasingly dense layers, defined by density stratification interfaces where the medium properties (e.g., temperature, salinity) change. The intensity of the stratification interfaces between the water column layers influences the internal mixing dynamics and entrainment (Cronin *et al.*, 2013; Qiu *et al.*, 2004), facilitating the transport of dissolved constituents, such as nutrients (Fu *et al.*, 2016), heat (de Lavergne *et al.*, 2014), oxygen (Keeling *et al.*, 2010; Breitburg *et al.*, 2018), pollutants, and carbon (DeVries *et al.*, 2017), over the vertical scales, ranging from microstructure to full ocean depth (Li *et al.*, 2020). The upper ocean stratification has been altered by human-induced climate change through increasing sea surface temperatures (Rhein *et al.*, 2013; Cabré *et al.*, 2015; Moore *et al.*, 2018; Yamaguchi and Suga, 2019; Li *et al.*, 2020), modification of storm patterns (Marsooli *et al.*, 2019), and larger river runoff (Graham, 2004). Quantifying the ocean stratification with high vertical resolution and across large areas is a necessary part of understanding the ocean, including its response to climate change.

Sonars (active acoustic systems) offer the opportunity for nonintrusive, synoptic observations of the water column, allowing for continuous, high resolution monitoring of the region over a broad spatial scale. High frequency (>10 kHz) acoustic systems have been used to collect informative datasets on the water column phenomena such as internal waves (Proni and Apel, 1975; Farmer and Smith, 1980; Sandstrom *et al.*, 1989; Orr *et al.*, 2000), the zooplankton community composition (Holliday and Pieper, 1995; Medwin and Clay, 1998), and a turbulence-induced oceanic microstructure (Munk and Garrett, 1973; Proni and Apel, 1975; Goodman and Kemp, 1981; Thorpe and Brubaker, 1983; Goodman, 1990; Seim *et al.*, 1995; Lavery *et al.*, 2003). The acoustic observations of stratification interfaces have been reported for decades (e.g., Barraclough *et al.*, 1969; Fisher and Squier, 1975; Penrose and Beer, 1981; Holbrook *et al.*, 2003). The recent studies with calibrated broadband acoustic systems have unequivocally linked the scattering observed at the stratification interface to changes in the water column density and sound speed (Stranne *et al.*, 2017; Stranne *et al.*, 2018; Weidner *et al.*, 2020). These studies have modeled the regions stratification as slightly rough surfaces and the inversion of these models has provided estimates of the stratification intensity (Shibley *et al.*, 2020). Although predicting the scattering from discrete layers is straightforward, through the use of the simple reflection coefficients (e.g., Kinsler *et al.*, 1999), when this same theory is applied to smooth gradients, it predicts no reflections.

Here, we present a model for describing the scattering from smooth stratification interfaces (e.g., no discontinuities in the first, second, etc. derivatives), which incorporates the characteristic scale of the interface as well as the frequency at which the interface is ensonified. The model, derived in Sec. II A, is based on the weak scattering model initially developed to describe the scattering from random perturbations in medium density and compressibility (Morse and Ingard, 1968), which is not specific to ocean stratification and could be applied in other cases for the scattering from

[a]Electronic mail: eweidner@ccom.unh.edu, ORCID: 0000-0001-9215-8697.

perturbations in weakly scattering media such as a turbulent oceanic microstructure or atmospheric turbulence-induced scattering of the electromagnetic waves (Morse and Ingard, 1968; Lavery *et al.*, 2003). The assumptions specific to oceanic stratification conditions are discussed in Sec. II B, where the importance of the acoustic forcing terms in the expression for the scattered pressure are defined for particular ocean environments. The final model expression is given in term of changes in the acoustic wave number (k), a function of the medium bulk modulus and density, to facilitate its application to ocean stratification interfaces.

II. SCATTERING FROM OCEANIC STRATIFICATION INTERFACES

In the following derivation of the model for the scattered pressure (p_s) from the stratification interface, we assume that the range (r) to the region of stratification is far from the source/receiver. Additionally, we assume that the stratification interface varies only in the r-direction. The result is an incident pressure wave (p_i), which appears locally planar, and a one-dimensional acoustic scattering model, a common approach for the scattering from discrete layers (e.g., Lavery and Ross, 2007).

A. Weak scattering by stratification interfaces

Consider a sound wave traveling through a fluid medium with a background density (ρ_0) and bulk modulus (β_0), which encounters a region of stratification at some range (r_d). The region of stratification is defined by a medium density (ρ_e) and bulk modulus (β_e), differing from the background values such that $\rho_e = \rho_0 + \delta_\rho$ and $\beta_e = \beta_0 + \delta_\beta$ (Fig. 1). These changes in the medium density and compressibility are assumed to be small compared to the background values such that $\delta_\rho/\rho_0 \ll 1$ and $\delta_\beta/\beta_0 \ll 1$.

The sound wave will be scattered from the changes in the medium arising from the stratification interface, and the nature of the scattered pressure can be described by the one-dimensional acoustic wave equation. Following steps that are similar to those outlined in Morse and Ingard (1968), we obtain an expression for the one-dimensional forced, reduced wave equation,

$$\frac{d^2}{dr^2}p_T(r) + {k_0}^2 p_T(r) = -{\delta_k}^2 p_T(r) + \frac{1}{\rho_0 + \delta_\rho}\frac{d\delta_\rho}{dr}\frac{d}{dr}p_T(r), \tag{1}$$

where $p_T(r)$ is the total pressure, and k_0 is the acoustic wave number of the background medium, a function of the angular frequency (ω) and speed of sound (c) ($k = \omega/c = \omega/\sqrt{\beta/\rho}$). ${\delta_k}^2$ is the total change in the squared acoustic wave number, arising from the stratification structure, which is defined as

$$\delta_k^2 = 2k_0\Delta k + \Delta k^2, \tag{2}$$

where Δk represents the change in the acoustic wave number between the background and stratification structure. A full derivation for Eq. (1) can be found in the Appendix.

Given that the changes in the medium density and bulk modulus are small compared to the background values, we assume a weakly scattering medium, where the Born approximation is valid, and define our complete model for the scattered pressure as

$$p_s(r) = \int\left[-\delta_k^2 p_i(r') + \frac{1}{\rho_0 + \delta_\rho}\frac{d\delta_\rho}{dr'}\frac{d}{dr'}p_i(r')\right]G(r|r')dr', \tag{3}$$

where r' is the range over the distributed source of scattering, in this case, the stratification structure, p_i is the incident pressure, p_s is the scattered pressure, and Green's function is defined for the one-dimensional wave as

$$G(r|r') = \frac{j}{2k_0}e^{-jk_0|r-r'|}. \tag{4}$$

B. Application to oceanic stratification structure

The scattered pressure defined in Eq. (3) is a function of two forcing terms, $-\delta_k^2 p_i(r')$ and $(1/\rho_0 + \delta_\rho)(d\delta_\rho/dr)(d/dr)p_i(r')$, which we will refer to as the sound speed forcing term and density gradient forcing term, respectively. The sound speed forcing term is defined by changes in acoustic wave number which, as noted previously, arises from changes in medium sound speed. Sound speed, a function of density and bulk modulus, is a commonly measured parameter in oceanography. The density gradient term is defined during the derivation of Eq. (1) when taking the divergence of the force equation, often referred to as the dipole term (see Morse and Ingard, 1968). The relative importance of these terms for the scattered pressure for a specific stratification interface will be defined by the environmental conditions unique to that location, specifically the local temperature, salinity, and their gradients over the stratification interface. The ratio of the forcing terms, $\zeta_{c\rho}$, describes their relative importance to the scattered pressure

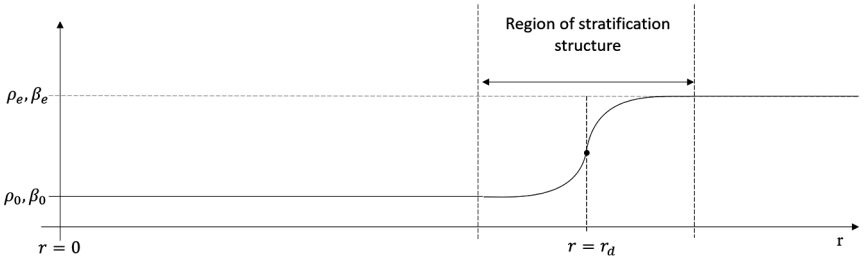

FIG. 1. The scattering geometry for a one-dimensional, far field, backscattering system, where an incident plane wave scatters from a region of stratification interface composed of changes in the density and bulk modulus. The profiles of the system density and bulk modulus along the vector r are shown. The stratification interface is centered at position $r = r_d$.

https://doi.org/10.1121/10.0009011

and can be explored for different ocean stratification conditions by evaluating

$$\zeta_{c\rho} = \delta_k^2 \Big/ \left(k_0 \frac{1}{\rho_0 + \delta_\rho} \frac{d\delta_\rho}{dr} \right) = \left(2k_0 \Delta k + \Delta k^2 \right) \Big/ \left(k_0 \frac{1}{\rho_0 + \delta_\rho} \frac{d\delta_\rho}{dr} \right), \quad (5)$$

where $k_0 = \omega/c_0$, $\Delta k = \omega/c_0 - \omega/c_e$, and $p_i(r)$ is assumed to be of the form $P_0 e^{-jk_0 r}$, such that $(d/dr)p_i(r) = -jk_0 p_i(r)$. The magnitude of Eq. (5) provides the means to evaluate the relative importance of these two terms on the scattered pressure.

To predict the relative importance of the perturbations in the sound speed and density gradients for the different oceanic conditions, five locations with strong, discrete stratification interfaces were identified from the literature (Table I): thermohaline staircase steps in the western tropical Atlantic (THSC-Tropics; Schmitt *et al.*, 2005), the Baltic Sea (THSC-Baltic; Weidner *et al.*, 2020), and the Arctic Ocean (THSC-Arctic; Stranne *et al.*, 2017), as well as the base of the mixed layer in the Baltic Sea (BML-Baltic; Weidner *et al.*, 2020) and the interface between a surface glacial meltwater layer and Fjord water in a high-latitude fjord (SGML-Fjord; Jakobsson *et al.*, 2014; Jakobsson *et al.*, 2020). These locations are regions in which the medium density and sound speed rapidly change because of intense stratification interfaces and are, therefore, likely candidates for strong acoustic scattering and model evaluation. They do not represent all of the cases of the oceanic stratification structure or the end member cases. The temperature and salinity gradients and the depth extent of the stratification interface reported in the literature for the test cases were used to calculate the environmental and perturbation densities and sound speed values using the Gibbs-SeaWater (GSW) Oceanographic Toolbox for MATLAB 2020a,[1] and those values were used to inform the forcing terms described in Eq. (5). Using the values from the literature, the relative importance of the forcing terms was computed for the five stratification test cases (Table I).

The sound speed forcing term dominates in almost all of the cases, and the relative impact of this term increases with the increasing frequency. In the lowest frequency example ($f_0 = 1$ kHz), for all of the environmental test cases except the surface glacial meltwater layer, the sound speed term is at least an order of magnitude greater than the density gradient forcing term. The only location where the magnitude of the density gradient term approaches that of the sound speed term is in the high-latitude fjord system, where a fresh layer of glacial meltwater sits atop the salty fjord water. There is minimal temperature contrast in this system, which is the stratification structure driven almost entirely by the salinity gradient; in this case, the two forcing terms approach each other in relative importance at low frequencies (<10 kHz). Nevertheless, the results suggest that the model for the scattered pressure [Eq. (3)] from the oceanic stratification interfaces can often be simplified by ignoring the contribution from the density gradient forcing term. This simplification breaks down in regions where there is strong, salinity-driven stratification and the frequencies of ensonification are low.

In addition to disregarding the density gradient forcing term, we can further simplify the model by ignoring the contribution in the sound speed forcing term from Δk^2. The relative importance of the two terms in the sound speed forcing term can be compared with the ratio

$$\zeta_k = 2k_0 \Delta k / \Delta k^2. \quad (6)$$

The ratio, ζ_k, was evaluated for all of the test cases (Table I) and in all of the cases, the Δk^2 term was several orders of magnitude smaller than the $2k_0\Delta k$ term. By ignoring the contributions to the scattered pressure from the density gradient forcing term and dropping Δk^2 from the sound speed forcing term, the model for the scattered pressure measured at the receiver can be simplified to

$$p_s(r = 0) = -j \int P_0 e^{-2jkr'} \Delta k dr', \quad (7)$$

where P_0 is the amplitude of the incident wave, the propagation direction of Green's function is written assuming $r > r'$, which would be the case for the backscatter, and the scattered pressure is measured at the source/receiver position ($r = 0$). The integral in Eq. (7) is the spatial Fourier transform of the disturbance, Δk, at half-wavelength scales as would be appropriate for the backscatter (i.e., the Bragg wave number), similar to that in previous work (e.g., Oeschger and Goodman, 1995).

Equation (7) is widely applicable to the horizontally flat regions of the sound speed change such as those in the oceanic echo sounding datasets from hull-mounted systems, in

TABLE I. The relative importance of the forcing terms in Eqs. (5) and 6 was determined from the fluid medium values for the temperature and salinity gradients (∇T, °C/m; ∇S, PSU/m), vertical extent of the stratification structure, Δz (m), and environmental and stratification density (ρ_0, ρ_e) and sound speed (c_0, c_e) values. $\zeta_{c\rho}$ was computed using an acoustic frequency range of 1–500 kHz; the first value reported for $\zeta_{c\rho}$ is for the 1 kHz case and the second value reported is for the 500 kHz case.

Case ID	∇T	∇S	Δz	ρ_0	ρ_e	c_0	c_e	$\zeta_{c\rho}$	ζ_k
THSC-Tropics	0.3	1.1	2	1029.6	1030.0	1488.2	1489.9	49.6/2.48e4	1.75e3
THSC-Baltic	1.15	1	1.3	1006.5	1008.8	1429.6	1437.7	28.3/1.42e4	354
THSC-Arctic	0.25	0.07	0.2	1028.1	1028.2	1442.7	1444.0	16.1/8.07e3	2.22e3
BML-Baltic	0.4	−0.25	1	1014.1	1013.9	1452.7	1454.0	39.2/1.96e4	2.24e3
SGML-Fjord	2.9	31.8	0.5	1001.6	1027.0	1421.2	1450.0	3.59/1.79e3	101

which the stratification interface is far from the projector/receiver and has minimal spatial variability relative to the ensonified area. However, in regions with strong salinity-driven stratification, such as estuaries or high-latitude fjords, neglecting the density gradient forcing term may lead to an underestimation of the scattering strength especially at low frequencies, and ζ_{cp} should be revisited in these cases.

III. DEFINING AN IDEALIZED ΔK PROFILE

To evaluate the model for the scattered pressure derived in Sec. II, the position and extent of the stratification interface relative to the acoustic projector/receiver must be defined. Additionally, the sound speed profile across the stratification interface as a function of the range from the projector/receiver should be defined to evaluate the Δk term in the integral of Eq. (7). The individual stratification interfaces in much of the Earth's oceans can be approximated as two-layer stratifications such as those illustrated in Fig. 1, in which a well-mixed upper layer is separated from a denser, homogeneous bottom layer by a thin region (Wessels and Hutter 1996; Michallet and Ivey, 1999). Taking into account the molecular diffusivity of the temperature and salinity, the structure would be a smooth interface between the two well-mixed bodies of water. Previous experiments have approximated the two-layer density distributions by a hyperbolic tangent profile (Troy and Koseff, 2005) and an error function profile (Thorpe 1971). Here, we describe the smooth stratification interface solely in terms of Δk with an inverse tangent functional form given as

$$\Delta k = \omega \frac{c_0 - c_e}{c_0 c_e}\left[\frac{1}{2} + \frac{1}{\pi}\tan^{-1}(a(r - r_d))\right], \tag{8}$$

where a defines the sharpness of the interface (i.e., the magnitude of the gradient between the layers). Equation (8) can used to evaluate the right-hand side of Eq. (7) to determine the scattered wave from the interface centered at r_d. Neglecting the non-propagating term, this results in the expression

$$p_s(r) = -\frac{j\omega}{\pi}\frac{c_0 - c_e}{c_0 c_e}\int P_0 e^{-2jkr'}\tan^{-1}(a(r - r_d))dr'. \tag{9}$$

Equation (9) is the Fourier transform of the inverse tangent function and simplifies to

$$p_s(r = 0) = -P_0\frac{c_0 - c_e}{2c_0}e^{-|2k/a|}e^{-2jkr_d}. \tag{10}$$

Equation (10) represents a frequency domain solution, and assuming that the incident wave can be represented by the Fourier transform pair $p_0 \leftrightarrow P_0$, the scattered wave in the time domain is given by

$$p_s(t, r = 0) = -\frac{c_0 - c_e}{2c_0}\int P_0 e^{-|2k/a|}e^{-2jkr_d}e^{j2\pi ft}df. \tag{11}$$

In the limit $a \to \infty$, the interface approaches the form of a discrete layer, the inverse tangent in Eq. (8) approaches $\pi/2$, the exponentially decaying term in Eqs. (10) and (11) approaches unity, and the expression for the scattered pressure becomes

$$p_s(t, r = 0) = -\frac{c_0 - c_e}{2c_0}\int P_0 e^{-2jkr_d}e^{j2\pi ft}df. \tag{12}$$

The resulting integral in Eq. (11) is a delayed version of the source waveform, where the delay is twice the distance to the sound speed anomaly, $2r_d/c$. The magnitude of the expression, $(c_0 - c_e)/2c_0$, is (to a good approximation) the reflection coefficient in the case where the density gradient term is negligible.

A. Frequency dependence of the scattered pressure

Equation (10) can be rearranged to give a reflection coefficient, $R = p_s/P_0$, whose amplitude is

$$|R| = \frac{|c_e - c_0|}{2c_0}e^{-|2k/a|}. \tag{13}$$

Equation (13) establishes a relationship between the sharpness of the interface (i.e., the magnitude of the gradient between the layers) and the frequency. If, for example, the intent is to find a frequency for which the difference in reflection between a discontinuous boundary ($a = \infty$) and a smooth boundary, such as that shown in Fig. 1, is 0.05 (5%), then

$$\frac{2k}{a} \le 0.05 \tag{14}$$

or

$$f_0 \le 0.05\frac{c}{4\pi}a. \tag{15}$$

Further, note that ~95% of the change between c_0 and c_e in Eq. (8) occurs for $-25/a < r < 25/a$. Using this as a measure of the width (L) of the stratification interface (see Fig. 1), Eq. (15) becomes

$$f_0 \le 0.05\frac{c_0}{4\pi}\frac{50}{L} \approx 0.2\frac{c_0}{L}. \tag{16}$$

Thus, to treat a smooth step such as that described by Eq. (8) as a sharp discontinuity, the gradient should have a spatial extent that is approximately 0.2λ or less. This condition is, obviously, harder to meet for the increasing frequencies: if a frequency f_0 exactly satisfies Eq. (15) such that the exponentially decaying term in Eq. (13) is 0.95, then this same term is 0.90 for $2f_0$, 0.82 for $4f_0$, 0.67 for $8f_0$, and so on, suggesting a gradual decay in the reflected wave amplitude with an increasing frequency (see Fig. 2). It may even be possible to match the frequency-dependent scattered wave amplitude to an exponential function to estimate L from the acoustic data alone provided that Eq. (8) was a good representation of the layer discontinuity and a wide range of frequencies was available.

https://doi.org/10.1121/10.0009011

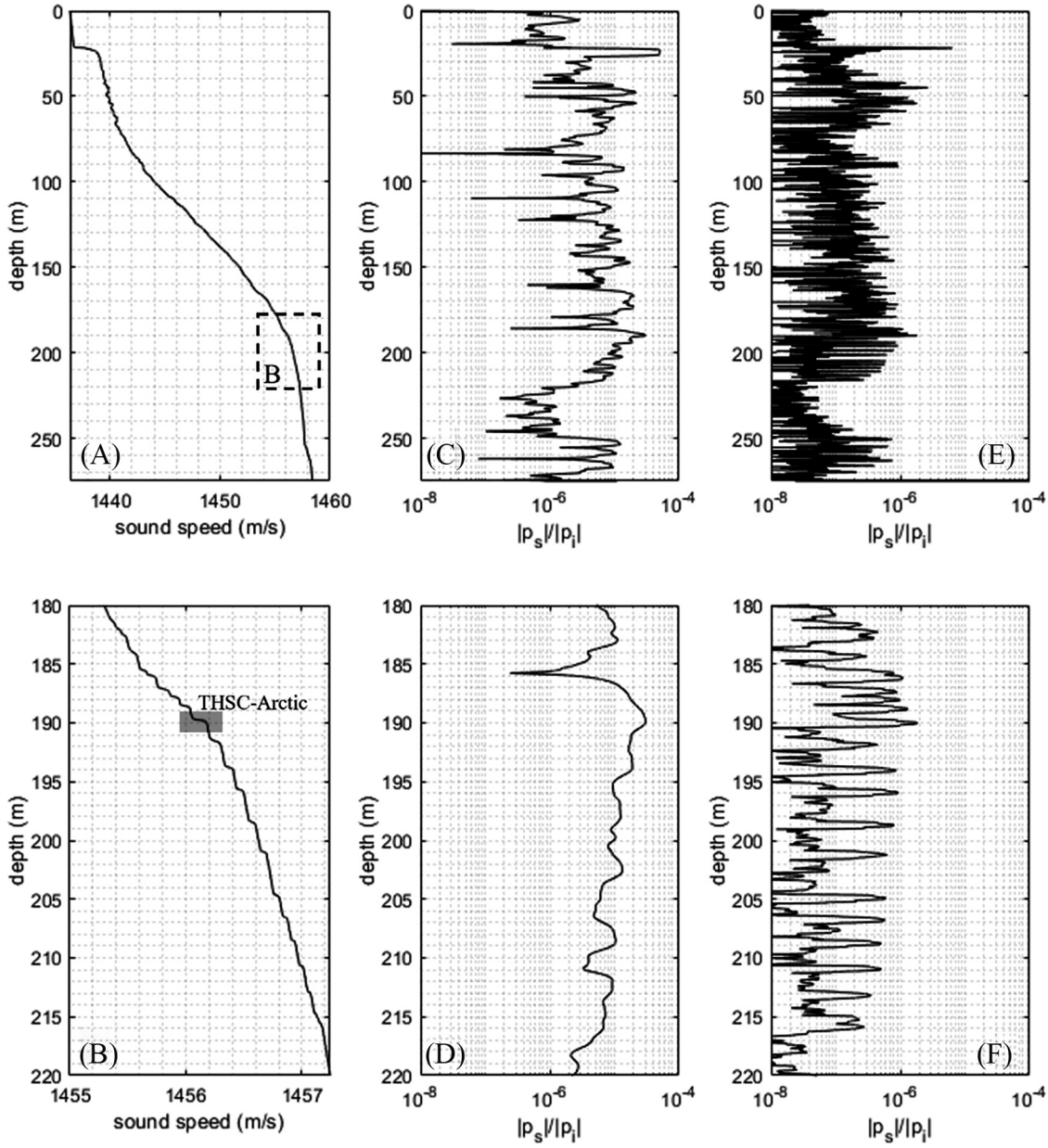

FIG. 2. (A) A vertical profile of the sound speed (m/s) from the upper water column of the central Arctic Ocean (Stranne *et al.*, 2017) is illustrated. The dashed box in (A) highlights the region of the thermohaline staircases structure and is shown in more detail in (B), The highlighted step in (B), marked "THSC-Arctic" is used for the idealized profile calculations found in Sec. IV A. The predicted acoustic reflections from the full water column and zoomed region of the thermohaline staircases are shown in (C)–(F). The model results described in Sec. IV B are depicted for the 2 kHz pulse in (C) and (D) and for the 20 kHz pulse in (E) and (F).

IV. MODELED PREDICTIONS FOR OCEANIC STRATIFICATION INTERFACES

In the ocean, weak scattered acoustic waves from a smooth interface, like those described in Sec. III A, may be observable in a number of ocean scenarios, including those examples from Sec. II: reflections from thermohaline staircases (Lavery and Ross, 2007; Stranne *et al.*, 2017; Weidner *et al.*, 2020) or high-latitude melt water lenses (Jakobsson *et al.*, 2014; Jakobsson *et al.*, 2020). Weak scattered waves may also be observable in other scenarios, including, for example, reflections from the boundary of the base of the mixed layer (Stranne *et al.*, 2018) or other stratification interfaces such as the permanent halocline (Ross and Lavery, 2012). Regardless of the underlying cause of the variation in the sound speed, a prediction of the scattered wave can be found using Eq. (7) after defining the nature of the stratification interface.

The stratification interface can be defined directly from the oceanographic data, such as conductivity, temperature, depth (CTD) profiles or high resolution microstructure data, collected *in situ*. In these datasets, CTD profilers or free-falling microstructure profiles collect discrete samples of the continuous physical properties of the water column, where the sampling frequency of the equipment determines the

vertical resolution of the resulting data set. From these *in situ* datasets of the water column temperature, conductivity (salinity), and depth, the vertical sound speed profile can be calculated using any number of oceanographic toolboxes such as the GSW toolbox1 or Seabird software.[2] Here, we define an *in situ* sound speed profile from a CTD cast collected in the Central Arctic Ocean, which defines the test case THSC-Arctic (Table I). The sound speed profile was used to numerically evaluate Eq. (10) to illustrate the potential scattered characteristics from the oceanic stratification interfaces (Fig. 2).

In Fig. 2, at a depth of approximately 25 m, there is a rapid increase in the sound speed, ∼3 m/s, associated with the base of the mixed layer. Additionally, between the depths of 180 and 230 m, there are a series of step-like features (thermohaline staircases). These staircases consist of a series of well-mixed layers separated by thin interfaces (∼5–10 cm), between which the sound speed increases between 0.1 and 0.3 m/s. The sound speed profile has a vertical resolution of 10 cm, defined by the CTD lowering speed and post-processing data density.

To apply the model for the scattered pressure, two definitions for Δk were defined and run through the model: (1) an idealized sound speed profile of an individual thermohaline staircase step defined by the THSC-Arctic case (Table I), which is explored in Sec. IV A, and (2) the numerical integration of the model for the full sound speed profile illustrated in Fig. 2, which is explored in Sec. IV B. Two acoustic pulses, one at 2 kHz and one at 20 kHz, were sent through the model space. Each pulse consisted of 15 cycles of a continuous wave complex sinusoid, weighted by a Tukey window with a 50% taper.

A. Idealized sound speed profile

An idealized sound speed profile was created using Eq. (11), the sound speed values outlined in Table I for the THSC-Arctic case, and an interface "sharpness factor" (a) of 347, such that the spatial extent of the discontinuity is 0.2λ at 2 kHz (Fig. 3). Using the sound speed step identified in Fig. 2, an idealized profile Δk was defined, and the model was evaluated using the acoustic pulses described above.

The acoustic backscattering results reflect the predictions made for the frequency dependence of the model in Sec. II A: the scattered wave looks like a delayed version of the source waveform and the scattering intensity is a function of the acoustic frequency. As the frequency of the acoustic pulse decreases, the magnitude of the scattered wave from the stratification interface increases and approaches the magnitude of the "idealized" reflection coefficient. In predicting the characteristics of the scattering waves from an idealized functional form of the sound speed profile described here, we assume the stratification is horizontally smooth.

B. *In situ* sound speed profile

The vertical resolution of the *in situ* sound speed profile was increased from the original 10 cm spacing to 0.01 m spacing using linear interpolation. Using the interpolated sound speed profile, the Δk profile was computed, and the acoustic scattering model was evaluated using the 2 and 20 kHz acoustic pulses described above (Fig. 2).

The results of the acoustic scattering in Fig. 2 show that the scattered wave from the 2 kHz pulse is considerably higher than the reflections from the 20 kHz pulse. The bottom of the mixed layer at a depth of ∼25 m causes, by far, the strongest reflection. There are several other locations with large reflections, including the region with the thermohaline staircases between 180 and 250 m. In this depth range, there are strong but unresolved reflections in the 2 kHz model output, whereas in the 20 kHz model output, the individual step features are resolved as individual

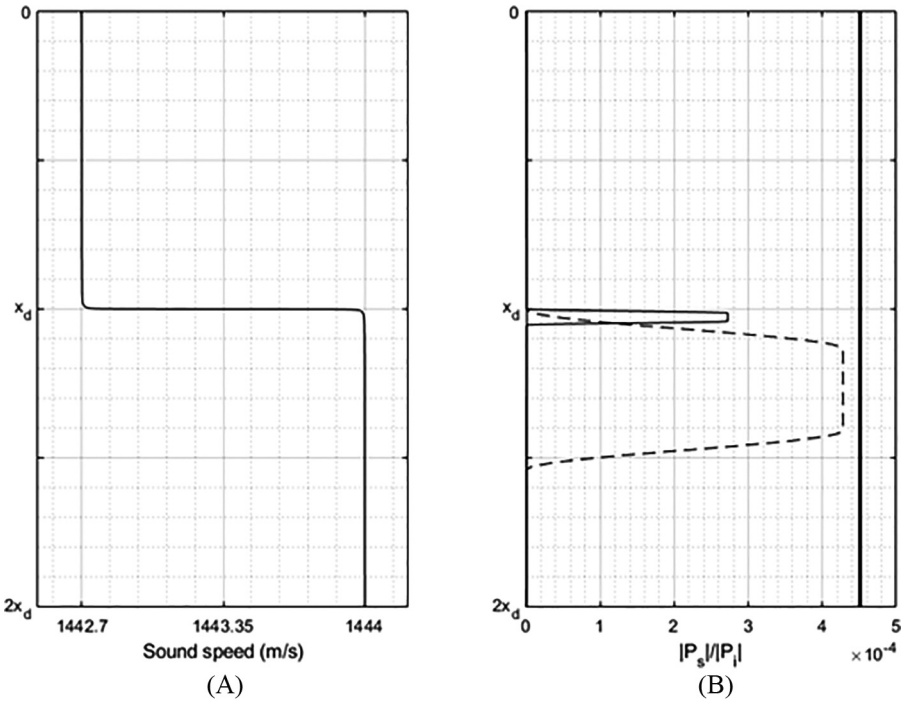

FIG. 3. In (A), a "step" change from a sound speed of 1442.7 to 1444.0 m/s with $a = 347$ is shown. In (B), the scattered pressure waves from the discontinuity for a 15 cycle sinusoid at 2 kHz (dashed line) and 20 kHz (thin solid line) are shown. The "ideal" reflection coefficient, in this case, equal to $R = 4.51e-4$ given by Eq. (13) when $a = \infty$, is shown as the thick black line in (B).

https://doi.org/10.1121/10.0009011

reflections. The results of our model indicate that the acoustic waves appear to be sensitive to small variations in the sound speed profile as observed in previous studies (e.g., Stranne *et al.*, 2017). This result suggests that high frequency acoustic systems could provide the means to explore the water column microstructure (<10 cm, depending on the frequency). This "acoustic microstructure probe" approach could provide high resolution information on the oceanic water column structure without the need for *in situ* data collection, although it will be important to differentiate the scattering from the stratification interfaces and other scattering mechanisms such as biology, turbulent microstructure, etc. It is worth noting that the resulting scattering profile assumes that the *in situ* sound speed profile captures all of the relevant changes in the sound speed from the stratification interfaces. For high frequencies, even high resolution microstructure profiles cannot provide *in situ* observations of the temperature and salinity structure at comparable spatial scales.

V. SUMMARY AND CONCLUSIONS

In this work, we have defined a one-dimensional acoustic scattering model for predicting the acoustic backscatter from the stratification interfaces, driven by changes in the medium density and sound speed, which is widely applicable to the acoustic data collected with ship-mounted sonars. Based on five typical oceanic stratification examples, we suggest that the scattering from the oceanic stratification interfaces will often be dominated by the wave number forcing term. The scattering from the density gradient forcing term can often be neglected. However, in regions with strong salinity-driven stratification, such as estuaries or high-latitude fjords, neglecting the density gradient term may lead to an underestimation of the scattering strength, particularly at low frequencies.

Our derivation of the acoustic scattering model presented in this work assumes that the Born approximation is valid, based on the far field, weak scattering assumptions. These assumptions require the density and sound speed perturbations arising from the stratification interface to be small compared to the background medium values and only vary as a function of the depth (range from the transceiver/receiver unit) with respect to the ensonified area. These assumptions will start to break down where the structure of the stratification interface diverges from the spatial homogeneity in cases where the strong external forcing (e.g., wind, tides) locally modifies the interface or in the presence of short period internal waves, which displace the interface vertically. In addition, the interfaces in which the changes in the medium sound speed and density are large, such as the air–sea or water–seabed interfaces, cannot be appropriately described with this model as they may violate the assumptions made in the derivation of the reduced, forced acoustic wave equation. Similarly, in the cases of strong salinity-driven stratification, such as estuaries or the high-latitude fresh water lens, the simplifications made in Sec. II B may start to break down, and the forcing caused by the density gradient term in Eq. (3) should be reconsidered.

We have made predictions for the scattered pressure based on an oceanographic sound speed profile collected in the central Arctic Ocean, containing stratification interfaces expressed as the base of the mixed layer near the surface and a series of thermohaline staircases deeper in the water column. Using the *in situ* sound speed profile, we numerically evaluated the model for the scattered pressure and determined that the acoustic waves are sensitive to small changes in the sound speed. The validity of these results is reinforced by the observations from previous acoustic studies of the ocean stratification structure with calibrated broadband backscatter data (e.g., Stranne *et al.*, 2017; Weidner *et al.*, 2020). In addition to the evaluation of this model for an *in situ* sound speed profile, we adopted an idealized function form for a typical central Arctic Ocean thermohaline staircase. The model predictions of the scattered pressure from the idealized form indicate the frequency-dependent scattering intensity based on the sharpness of the stratification interface as anticipated from the derivation. Using this model, the broadband acoustic inversion could provide high resolution, remote estimations of the physical water column properties of the oceanic stratification. This model can be used to build on the previous acoustic inversion efforts of the ocean stratification structure (e.g., Shibley *et al.*, 2020) by considering the vertical extent of the interface and frequency-dependent scattering. Combining the measurements from the acoustic inversion efforts with the existing *in situ* observational platform, such as gliders and buoys (Qiu *et al.*, 2004; Boyer *et al.*, 2013), as well as the publicly available worldwide datasets ocean temperature (T) and salinity (S) profiles such as The World Ocean Database (Boyer et al., 2013), will allow for the quantification of the ocean stratification with a high vertical resolution and across large areas. The broadband acoustic measurements can provide the information necessary for the interpolation between profiles and provide the spatial coverage necessary to describe the oceanic stratification interfaces across basins and the actively evolving temporal and spatial changes in the stratification due to the ongoing climate change.

ACKNOWLEDGMENTS

The authors would like to thank Christian Stranne (Geological Sciences Department, Stockholm University) for providing the oceanographic sound speed profile from the Central Arctic Ocean. This work was supported, in part, by the National Oceanic and Atmospheric Administration Award No. NA15NOS4000200.

APPENDIX: DERIVATION OF THE FORCED, REDUCED WAVE EQUATION

To model the backscattering from the changes in the density and bulk modulus brought about by the stratification interfaces, we must incorporate the perturbations from the

acoustic wave and the environmental inhomogeneity into our derivation of the acoustic wave equation. We follow the derivation of the forced, reduced wave equation from Morse and Ingard (1968). This derivation deviates from that of Morse and Ingard (1968) at Eq. (8.1.10) to define the final expression in terms of the acoustic wave number rather than the compressibility.

Equation (A1) is identical to Eq. (8.1.10) in Morse and Ingard (1968) after substituting the medium bulk modulus (β_0) for the compressibility,

$$-\frac{1}{\beta_0+\delta_\beta}\frac{\partial p}{\partial t}+\nabla\left(\frac{1}{\rho_0+\delta_\rho}\nabla p\right)=0, \tag{A1}$$

where δ_β is the perturbation in the bulk modulus away from the medium background values, and δ_p is the density perturbation brought about by the acoustic wave's pressure (p). The expansion of Eq. (A1) results in

$$-\frac{1}{\beta_0+\delta_\beta}\frac{\partial p}{\partial t}+\frac{1}{\rho_0+\delta_\rho}\nabla^2 p+\nabla\left(\frac{1}{\rho_0+\delta_\rho}\right)\nabla p=0. \tag{A2}$$

Taking the divergence of the $(\rho_0+\delta_\rho)^{-1}$ term in Eq. (A2) and multiplying by both sides by $(\rho_0+\delta_\rho)$ results in

$$\nabla^2 p+{k_e}^2\frac{\partial p}{\partial t}=\frac{\nabla\delta_\rho}{\rho_0+\delta_\rho}\nabla p, \tag{A3}$$

where ${k_e}^2=(\rho_0+\delta_\rho)/(\beta_0+\delta_\beta)={k_0}^2+{\delta_k}^2$, and from this expression and Eq. (A2), the final expression for the acoustic wave equation in Eq. (1) can be reached.

[1]See http://www.teos-10.org/ (Last viewed 06/30/2021).
[2]See https://www.seabird.com/ (Last viewed 06/30/2021).

Barraclough, W. E., Le Brasseur, R. J., and Kennedy, O. D. (**1969**). "Shallow scattering layer in the subarctic Pacific Ocean: Detection by high frequency echo sounder," Science **166**, 611–613.

Breitburg, D., Levin, L. A., Oschlies, A., Grégoire, M., Chavez, F. P., Conley, D. J., Garçon, V., Gilbert, D., Gutiérrez, D., Isensee, K., Jacinto, G. S., Limburg, K. E., Montes, I., Naqvi, S. W. A., Pitcher, G. C., Rabalais, N. N., Roman, M. R., Rose, K. A., Seibel, B. A., Telszewski, M., Yasuhara, M., and Zhang, J. (**2018**). "Declining oxygen in the global ocean and coastal waters," Science **359**, eaam7240.

Boyer, T. P., Antonov, J. I., Baranova, O. K., Coleman, C., Garcia, H. E., Grodsky, A., Johnson, D. R., Locarnini, R. A., Mishonov, A. V., O'Brien, T. D., Paver, C. R., Reagan, J. R., Seidov, D., Smolyar, I. V., and Zweng, M. M. (**2013**). "World ocean database 2013," in *NOAA Atlas NESDIS*, edited by S. Levitus and A. Mishonov(NESDIS, Silver Springs, MD), Vol. 72, p. 209.

Cabré, A., Marinov, I., and Leung, S. (**2015**). "Consistent global responses of marine ecosystems to future climate change across the IPCC AR5 Earth system models," Clim. Dyn. **45**, 1253–1280.

Cronin, M. F., Bond, N. A., Farrar, J. T., Ichikawa, H., Jayne, S. R., Kawai, Y., Konda, M., Qiu, B., Rainville, L., and Tomita, H. (**2013**). "Formation and erosion of the seasonal thermocline in the Kuroshio Extension recirculation gyre," Deep-Sea Res. **85**, 62–74.

de Lavergne, C., Palter, J. B., Galbraith, E. D., Bernardello, R., and Marinov, I. (**2014**). "Cessation of deep convection in the open Southern Ocean under anthropogenic climate change," Nat. Clim. Change **4**, 278–282.

DeVries, T., Holzer, M., and Primeau, F. (**2017**). "Recent increase in oceanic carbon uptake driven by weaker upper-ocean overturning," Nature **542**, 215–218.

Farmer, D. M., and Smith, J. D. (**1980**). "Tidal interaction of stratified flow with a sill in Knight Inlet," Deep-Sea Res., Part A **27**, 239–254.

Fisher, F. H., and Squier, E. D. (**1975**). "Observation of acoustic layering and internal waves with a narrow-beam 87.5-khz echo sounder," J. Acoust. Soc. Am. **58**, 1315–1317.

Fu, W., Randerson, J. T., and Moore, J. K. (**2016**). "Climate change impacts on net primary production (NPP) and export production (EP) regulated by increasing stratification and phytoplankton community structure in the CMIP5 models," Biogeosciences **13**, 5151–5170.

Graham, L. P. (**2004**). "Climate change effects on river flow to the Baltic Sea," Ambio **33**, 235–241.

Goodman, L. (**1990**). "Acoustic scattering from ocean microstructure," J. Geophys. Res. **95**, 11557–11573.

Goodman, L., and Kemp, K. A. (**1981**). "Scattering from volume variability," J. Geophys. Res. **86**, 4083–4088, https://doi.org/10.1029/JC086iC05p04083.

Holbrook, W. S., Páramo, P., Pearse, S., and Schmit, R. W. (**2003**). "Thermohaline fine structure in an oceanographic front from seismic reflection profiling," Science **301**, 821–824.

Holliday, D. V., and Pieper, R. E. (**1995**). "Bioacoustical oceanography at high frequencies," ICES J. Mar. Sci. **52**, 279–296.

Jakobsson, M., Hogan, K. A., Mayer, L. A., Mix, A., Jennings, A., Stoner, J., Eriksson, B., Jerram, K., Mohammad, R., Pearce, C., Reilly, B., and Stranne, C. (**2014**). "The Holocene retreat dynamics and stability of Petermann Glacier in northwest Greenland," Nat. Commun. **9**, 2104.

Jakobsson, M., Mayer, L., Nilsson, J., Stranne, C., Calder, B., O'Regan, M., Brüchert, V., Chawarski, J., Cronin, T. M., Eriksson, B., Farell, J., Fredriksson, J., Gemery, L., Glueder, A., Handl, T., Holmes, F. A., Jerram, K., Kirchner, N., Mix, A., Muchowski, J., Padman, J., Prakash, A., Reed, S., Reilly, B., Ståhl, E., Ulfsbo, A., Weidner, E., West, G., and Åkesson, H. (**2020**). "Ryder Glacier in northwest Greenland is shielded from warm Atlantic water by a bathymetric sill," Commun. Earth Environ. **1**(45), 1–10.

Keeling, R. F., Körtzinger, A., and Gruber, N. (**2010**). "Ocean deoxygenation in a warming world," Annu. Rev. Mar. Sci. **2**, 199–229.

Kinsler, L. E., Frey, A. R., Coppens, A. B., and Sanders, J. V. (**1999**). *Fundamentals of Acoustics*, 4th ed. (Wiley, New York).

Lavery, A., and Ross, T. (**2007**). "Acoustic scattering from double-diffusive microstructure," J. Acoust. Soc. Am. **122**, 1449–1462.

Lavery, A. C., Schmitt, R. W., and Stanton, T. K. (**2003**). "High-frequency acoustic scattering from turbulent oceanic microstructure: The importance of density fluctuations," J. Acoust. Soc. Am. **114**(5), 2685–2697.

Li, G., Cheng, L., Zhu, J., Trenberth, K. E., Mann, M. E., and Abraham, J. P. (**2020**). "Increasing ocean stratification over the past half-century," Nat. Clim. Change **10**, 1116–1123.

Marsooli, R., Lin, N., Emanuel, K., and Feng, K. (**2019**). "Climate change exacerbates hurricane flood hazards along US Atlantic and Gulf Coasts in spatially varying patterns," Nat. Commun. **10**, 1–9.

Medwin, H., and Clay, C. S. (**1998**). *Fundamentals of Acoustical Oceanography* (Academic, New York).

MIchallet, H., and Ivery, G. N. (**1999**). "Experiments on mixing due to internal solitary waves breaking on a uniform surface," J. Geophys. Res. **104**(C6), 13467–13478, https://doi.org/10.1029/2021JC017275.

Moore, J. K., Fu, W., Primeau, F., Britten, G. L., Lindsay, K., Long, M., Doney, S. C., Mahowald, N., Hoffman, F., and Randerson, J. T. (**2018**). "Sustained climate warming drives declining marine biological productivity," Science **359**(6380), 1139–1143.

Morse, P. M., and Ingard, K. U. (**1968**). *Theoretical Acoustics* (Princeton University Press, Princeton, NJ), p. 262, pp. 407–409.

Munk, W. H., and Garrett, C. J. R. (**1973**). "Internal wave breaking and microstructure," Boundary-Layer Meteorol. **4**, 37–45.

Oeschger, J., and Goodman, L. (**1995**). "Acoustic scattering from a thermally driven buoyant plume," J. Acoust. Soc. Am. **100**, 1421–1462.

Orr, M. H., Haury, L. R., Wiebe, P. H., and Briscoe, M. G. (**2000**). "Backscatter of high-frequency ~200 kHz acoustic wave fields from ocean turbulence," J. Acoust. Soc. Am. **108**, 1595–1601.

Penrose, J. D., and Beer, T. (**1981**). "Acoustic reflection from estuarine pycnoclines," Estaurine Coastal Shelf Sci. **12**, 237–249.

Proni, J. R., and Apel, J. R. (**1975**). "On the use of high-frequency acoustics for the study of internal waves and microstructure," J. Geophys. Res. **80**, 1147–1151, https://doi.org/10.1029/JC080i009p01147.

Qiu, B., Chen, S., and Hacker, P. (**2004**). "Synoptic-scale air–sea flux forcing in the western North Pacific: Observations and their impact on SST and the mixed layer," J. Phys. Ocean. **34**, 2148–2159.

Rhein, M., Rintoul, S. R., Aoki, S., Campos, E., Chambers, D., Feely, R. A., Gulev, S., Johnson, G. C., Josey, S. A., Kostianoy, A., Mauritzen, C., Roemmich, D., Talley, L. D., and Wang, F. **2013**). "Observations: Ocean," in *Climate Change 2013: The Physical Science Basis. Contribution of Working Group I to the Fifth Assessment Report of the Intergovernmental Panel on Climate Change, Observations: Ocean*, edited by T. F. Stocker and reviewed by H. Freeland, S. Garzoli, and Y. Nojiri (Cambridge University Press, Cambridge, UK), Chap. 3.

Ross, T., and Lavery, A. C. (**2012**). "Acoustic scattering from density and sound speed gradients: Modeling of oceanic pycnoclines," J. Acoust. Soc. Am. **131**, EL54.

Sandstrom, H., Elliott, J. A., and Cochrane, N. A. (**1989**). "Observing groups of solitary internal waves and turbulence with BATFISH and Echo-Sounder," J. Phys. Oceanogr. **19**, 987–997.

Schmitt, R. W., Ledwell, J. R., Montgomery, E. T., Polzin, K. L., and Toole, J. M. (**2005**). "Enhanced diapycnal mixing by salt fingers in the thermocline of the tropical Atlantic," Science **308**, 685–688.

Seim, H. E., Gregg, M. C., and Miyamoto, R. T. (**1995**). "Acoustic backscatter from turbulent microstructure," J. Atmos. Ocean. Technol. **12**, 367–380.

Shibley, N., Timmermans, M. L., and Stranne, C. (**2020**). "Analysis of acoustic observations of double-diffusive finestructure in the Arctic Ocean," Geophys. Res. Lett. **47**, e2020GL089845, https://doi.org/10.1029/2020GL089845.

Stranne, C., Mayer, L., Jakobsson, M., Weidner, E., Jerram, K., Weber, T. C., Anderson, L. G., Nilsson, J., Björk, G., and Gårdfeldt, K. (**2018**). "Acoustic mapping of mixed layer depth," Ocean Sci. **14**, 503–514.

Stranne, C., Mayer, L., Weber, T. C., Ruddick, B. R., Jakobsson, M., Jerram, K., Weidner, E., Nilsson, J., and Gårdfeldt, K. (**2017**). "Acoustic mapping of thermohaline staircases in the Arctic Ocean," Sci. Rep. **7**, 1–9.

Thorpe, S. A. (**1971**). "Experiments on the instability of stratified shear flows: Miscible fluids," J. Fluid Mech. **46**, 299–319.

Thorpe, S. A., and Brubaker, J. M. (**1983**). "Observation of sound reflection by temperature microstructure," Limnol. Oceanogr. **28**, 601–613.

Troy, C. D., and Koseff, J. R. (**2005**). "The instability and breaking of long internal waves," J. Fluid Mech. **543**, 107–136.

Weidner, E., Stranne, C., Hentati, J. S., Weber, T. C., Mayer, L., and Jakobsson, M. (**2020**). "Tracking the spatiotemporal variability of the oxic–anoxic interface in the Baltic Sea with broadband acoustics," ICES J. Mar. Sci. **77**(7-8), 2814–2824.

Wessels, F., and Hutter, K. (**1996**). "Interaction of internal waves with a topographic sill in a two-layered fluid," J. Phys. Oceanogr. **26**, 5–20.

Yamaguchi, R., and Suga, T. (**2019**). "Trend and variability in global upper-ocean stratification since the 1960s," J. Geophys. Res.: Oceans **124**, 8933–8948, https://doi.org/10.1029/2019JC015439.